Journal of Sound and Vibration (1999) **226**(1), 1–23
Article No. jsvi.1999.2211, available online at http://www.idealibrary.com on IDEAL®

OPTIMUM SHAPE DESIGN AGAINST FLUTTER OF A CANTILEVERED COLUMN WITH AN END-MASS OF FINITE SIZE SUBJECTED TO A NON-CONSERVATIVE LOAD

MIKAEL A. LANGTHJEM† AND YOSHIHIKO SUGIYAMA

Department of Aerospace Engineering, Osaka Prefecture University, Sakai-shi, Osaka 599-8531, *Japan*

(*Received* 3 *June* 1998, *and in final form* 20 *January* 1999)

Optimum design for dynamic stability of slender cantilevered columns subjected to a follower force, due to a rocket thrust, is investigated. The aim is to determine the tapering of the column which maximizes the critical value of the rocket thrust (at which flutter is initiated) under the constraint of constant length and volume of the column. The rocket thrust is assumed to be produced by a solid rocket motor mounted at the tip end of the column. The rocket motor is simplified as a massive ball with the same material density as the column. Based on experimental evidence [1,2] it is argued that a mathematical model without damping gives the practical stability limit if internal and external damping is small and the rocket thrust acts only in a short interval of time. Optimum columns are determined for various sizes of the end-ball (rocket motor). For small sizes, the critical thrust can be significantly increased by optimization, about eight times. By practical (experimental realizable) values of the mass ratio $\mu =$ (mass of end-ball)/(mass of column) the critical thrust can only be increased 1·3–1·4 times which is similar to the case of a pure conservative (dead) end load. Also, it is found that the great sensitivity to small changes in design parameters, which significantly complicates optimization of the pure Beck's column, is not present for practical values of μ. It is argued then, that the 'pure' Beck's column should be considered as a theoretical limit case of vanishing end-mass.

1. INTRODUCTION

A classical 'model problem' within the field of dynamic stability is Beck's column—a cantilevered column subjected to a so-called 'follower force' at the free end [3, 4]. The line of action of this force always remains tangential to the deformed beam axis at the free end. The load is thus *non-conservative* and the column is subject to dynamic instability (flutter). It is important to obtain a full understanding

†Current address: Institue of Mechanical Engineering, Aalborg University, Pontoppidanstraede 101, DK-9220 Aalborg East, Denmark.

0022-460X/99/360001 + 23 $30.00/0

of dynamic stability in order to prevent its occurrence in, for example, aircraft and aerospace structures. Many theoretical studies have been carried out, especially on the effect of damping, but only few have been followed up by experiments. One reason may be that it is very difficult to produce and control a pure follower force in the laboratory. Consequently, studies on follower force systems have from time to time been severely criticized as being out of touch with reality (e.g. reference [5], but see also references [6, 7]). A flexible, cantilevered fluid-conveying tube, where the fluid is discharged at the free end, is an example of another system subjected to a follower force (due to the momentum flux at the free end). This system, which can easily be realized, is however also subjected to gyroscopic forces due to moving mass of flowing fluid and to significant fluid damping. In many practical problems, especially in aerospace applications, the damping is very small. However, it is known that the theoretical flutter limits are very different in the cases of no damping and small internal (material) damping [3, 4]. Beck's problem was realized in almost pure form by Sugiyama *et al.* [1]. It was done by installing a small solid rocket motor at the free end of a cantilevered column. This experimental study verified the flutter instability and clarified the effect of damping.

In [1] Sugiyama *et al.* compare the stability limits obtained (i) experimentally, (ii) theoretically with inclusion of internal and external damping and (iii) theoretically with neglect of both types of damping. The conclusion is that the stability curve calculated with neglect of damping agrees well with the experiments, while the curve calculated with inclusion of (internal and external) damping significantly underestimates the stability limit. This can be understood by considering the behaviour of the leading eigenvalues (those having largest real parts) in an $\mathrm{Re}(\lambda) - \mathrm{Im}(\lambda)$ diagram. We will consider vibrations of the form

$$a(x)\exp(\lambda t), \tag{1}$$

where $a(x)$ is the amplitude and $\lambda = \sigma + \mathrm{i}\omega$ is a complex eigenvalue. As just mentioned, the critical load for the damped model, p_{damped} say, is significantly lower than the critical load for the undamped model, $p_{undamped}$. [Roughly, $p_{damped} \approx p_{undamped}/2$.] But in the load interval $p_{damped} < p < p_{undamped}$ the 'unstable eigenvalue', which has a small positive value of σ, is *creeping* along the $\mathrm{Re}(\lambda)$-axis if both internal and external damping is very small. This is the case for a slender metal rod (e.g., aluminium) vibrating in air. So, although the system mathematically (in the sense of Lyapunov) of course is unstable, the growth-rate of the unstable vibrations is so small that the system from an experimental point of view will appear to be stable within the burning time of the rocket motor, which typically is just 3–4 s.

This problem was foreseen and discussed already in 1965 by Hermann and Jong [8], who proposed a relaxed stability criterion based on a measure of the rate of amplitude-growth during one period of oscillation. Sugiyama *et al.* [1] suggested a slightly different stability criterion, namely: the system is considered stable if small disturbances are amplified less than n times during the burning time of the rocket motor (which was 4 s in their experiments). From equation (1) it is seen that, if the burning time is t_b and the largest σ-value is $\sigma_{\max}$, the system is considered as being

stable if

$$\exp(\sigma_{\max} t_b) < n. \tag{2}$$

The critical load, p_{cr} say, is thus defined as the load at which

$$\sigma_{\max} = \frac{\ln(n)}{t_b}. \tag{3}$$

To exemplify, for one of the experiments in reference [1], the 'practical' stability criterion gives, with $n = 10$, a non-dimensional critical load p_{cr} of magnitude 12·61. This value is not very different from the theoretical value 12·60 obtained by neglecting damping, but certainly very different from the theoretical value 5·65 obtained by including damping. [On the other hand, if the rocket burning time t_b is not such a short period of time, $\sigma_{\max}$ must necessarily be very small. As $t_b \to \infty$, p_{cr} smoothly approaches p_{damped}.]

The undamped mathematical model then gives, to a very good approximation, the 'practical' stability limit if the damping is small and the follower force is applied only in a short interval of time. This has been re-evaluated now in a number of experiments [2]. It is worth remarking that this is also the conclusion of the 1990 review paper "Destabilizing paradox in stability problems of non-conservative systems" by Seyranian [9] who writes, "The destabilizing paradox due to infinitesimal damping is of a formal nature and it is the consequence of the use of the stability criterion on an infinite interval of time. When damping tends to zero, then the formal limit of the critical value looses the physical meaning of boundary of vibrational stability; the critical parameter of the system with zero damping is the boundary of practical stability."

It must be emphasized that the above discussion assumes that the disturbances are so small that non-linear effects do not come into play and change the stability limit predicted by a linear analysis. Considering the already mentioned cantilevered fluid-conveying tube, experiments show that long, slender tubes remain stable to large disturbances when the flow-rate is just below the critical value. Relatively short tubes, on the other hand, are only stable to a small disturbance (a 'snap' by a finger). A larger disturbance (a strong push) may initiate limit-cycle motion [10]. [In the first case, the flutter boundary is characterized by a supercritical bifurcation; in the latter case by a subcritical bifurcation.] Similar phenomena may be expected for the present system.

Large space structures may be maneuvered in space by means of pusher-type rocket motors (which are active in short intervals of time only). For such structures, optimum design against dynamic instability is of major importance. Typically, the optimization problem is formulated as (a) for a fixed critical load p_{cr}, determine the structure of least weight or, (b) for a given amount of material (weight), determine the strongest structure, i.e., the structure with the largest critical load p_{cr}. In the development of efficient and robust optimization methods for non-conservative problems, Beck's problem has been used as a 'model problem' for many years [11–15]. The critical (flutter) load of Beck's column can be increased significantly

by optimization, 6–8 times larger than for a uniform column, both with and without inclusion of damping [16]. For comparison, the critical (buckling) load for a cantilevered column subjected to a conservative (dead) load can only be made 1·33 times larger by optimization [17].

Previous papers on the optimum design of Beck's column have focused on the numerical optimization method and no attention has been paid to the physical realization and experimental verification of the results. The aim of the present paper is to determine the optimum tapering of cantilevered columns subjected to a tangential follower force, due to the thrust produced by an end-mounted rocket motor. This is done with an experimental verification of the optimum design in mind which is particularly interesting since apparently, the optimally shaped Beck's column is so very much more 'efficient' than the corresponding uniform column. A column with circular cross-sections is considered in this paper such that direct comparison with previous theoretical work, such as reference [15], is possible.

Concerning the planned experimental verification of the effect of optimization, care will be taken to make sure that the vibrations occur in one plane only. This is most easily obtained by using beams with rectangular cross-sections. Figure 1 shows the experimental setup with an optimally shaped aluminium beam. The small solid-propellant rocket motors are specially manufactured by Daicel Chemical Industries, Ltd. Great care must be taken to obtain a well-defined and uniform thrust during the whole burning time. The motors are thus very costly and so far, only a couple of test-runs have been made with optimally shaped columns. The experiments will be described in a future paper.

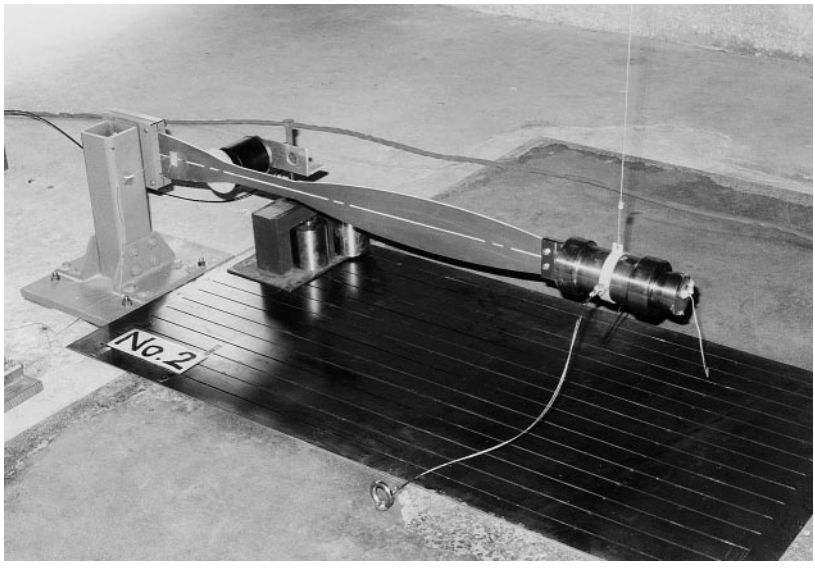

Figure 1. A general view of the experimental setup of an optimally shaped aluminium column, with rectangular cross-sections, subjected to a rocket thrust at the free end.

The present paper is divided into six sections. Section 2 deals with the stability analysis. For simplicity, the column is treated as a Bernoulli–Euler beam in this paper. Ryu and Sugiyama [18] studied the influence of rotatory inertia and shear deformation of the column for a similar model. They concluded that these corrections to the simple beam model hardly affect the flutter load of slender columns but the rotatory inertia and the finite size of the rocket motor (end-ball) cannot be neglected. In section 3, the influence of the size of the end-ball on the stability limit and on the flutter oscillations of uniform columns is discussed. Section 4 describes the optimization problem and the numerical method. The numerical results are discussed in section 5. It is suggested that the case of no end-mass (Beck's column) should be considered as the theoretical limit case since the optimum design has vanishing tip cross-section area. This means that the curvature of the column can become extremely large at the free end during the flutter oscillations. Figure 6(a) shows that this is indeed the case. The critical load of this column significantly exceeds that of a uniform column with same length and volume, almost eight times. By taking the, in praxis unavoidable, end-mass into consideration, the optimization gain factor $p_{cr}^{optimal}/p_{cr}^{uniform}$ is significantly reduced and the curvature at the free end of the column becomes much more reasonable, see Figure 6. By a mass ratio (mass of end-ball)/(mass of column) which resembles those realized by Sugiyama *et al.* [1, 2], the gain factor is only about 1·3, similar to what can be obtained in the case of a purely conservative load. By continued increase of the mass ratio the gain factor is not reduced but remains almost constant. The main conclusions are summarized in section 6.

2. STABILITY ANALYSIS

2.1. DIFFERENTIAL EQUATION AND BOUNDARY CONDITIONS

The system under investigation is sketched in Figure 2(a) and its mathematical idealization in Figure 2(b). The mathematical model consists of a cantilevered column, of length L, with a ball at the free end. It will be assumed that the column has circular cross-setions with radius $r = r(x)$. The material density is denoted by ρ. The ball represents a solid rocket motor which, by its thrust, provides the follower force p. If the radius of the ball is denoted by a and its density also is ρ (as the column), it has the mass

$$M = \tfrac{4}{3}\pi\, a^3\rho \tag{4}$$

and rotatory inertia

$$J = \tfrac{2}{5}\, M\, a^2 = \tfrac{8}{15}\pi\, a^5\rho \tag{5}$$

about an axis through its centre. Rotatory inertia and shear effects of the column are ignored in the present study. Damping is ignored in accordance with the discussion in section 1. Small-amplitude vibrations around the trivial equilibrium

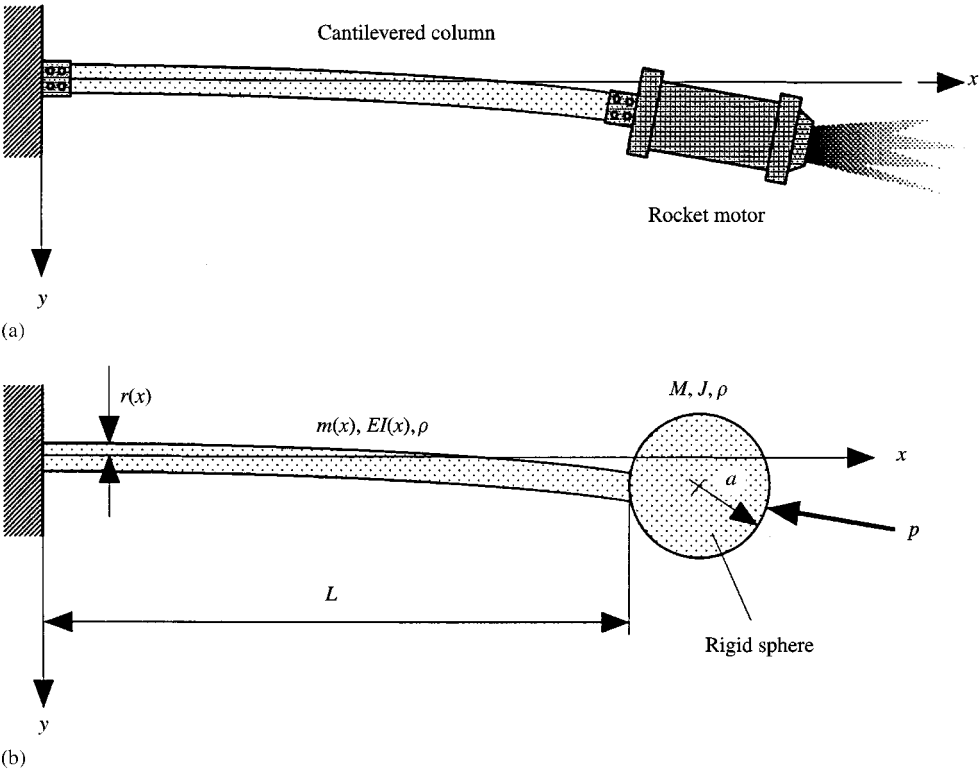

Figure 2. (a) Cantilevered column subjected to a follower force, realized by the thrust of an end-mounted rocket motor; (b) Mathematical model. Sketch of the idealized system.

configuration are then governed by the linear differential equation

$$\frac{\partial^2}{\partial x^2}\left\{EI(x)\frac{\partial^2 y}{\partial x^2}\right\} + p\frac{\partial^2 y}{\partial x^2} + m(x)\frac{\partial^2 y}{\partial t^2} = 0, \tag{6}$$

where x is the length parameter, t is the time, y is the lateral displacement, E is the modulus of elasticity, $I(x)$ is the area moment of inertia, $m(x) = \rho\pi r(x)^2$ is the mass distribution and p is the follower load. The boundary conditions are [1]

$$y = 0 \quad \text{and} \quad \frac{\partial y}{\partial x} = 0 \qquad \text{at } x = 0,$$

$$EI\frac{\partial^2 y}{\partial x^2} + M\frac{\partial^2}{\partial t^2}\left(y + a\frac{\partial y}{\partial x}\right)a + J\frac{\partial^3 y}{\partial x \partial t^2} = 0 \text{ and}$$

$$\frac{\partial}{\partial x}\left\{EI\frac{\partial^2 y}{\partial x^2}\right\} - M\frac{\partial^2}{\partial t^2}\left(y + a\frac{\partial y}{\partial x}\right) = 0 \quad \text{at } x = L. \tag{7}$$

The time-dependence is assumed to be of the form

$$y(x, t) = \bar{y}(x)\exp(\tilde{\lambda}t), \quad \tilde{\lambda} = \tilde{\sigma} + \mathrm{i}\tilde{\omega}. \tag{8}$$

In order to obtain a dimensionless formulation, the following dimensionless parameters are defined:

$$\bar{x} = \frac{x}{L}, \quad \bar{y} = \frac{y}{L}, \quad \zeta = \frac{r_0}{L}, \quad \kappa = \frac{a}{r_0}, \quad \lambda = \tilde{\lambda}\frac{t}{\bar{t}} = \sigma + \mathrm{i}\omega,$$

$$\bar{t} = \frac{t}{L^2}\sqrt{\frac{EI_0}{m_0}}, \quad \bar{p} = \frac{pL^2}{EI_0}, \quad \bar{m}(\bar{x}) = \frac{m(x)}{m_0}, \quad \bar{s}(\bar{x}) = \frac{I(x)}{I_0}. \tag{9}$$

Quantities with index "0" refer to a specified uniform column. By using that $\bar{s}(\bar{x}) = (\bar{m}(\bar{x}))^2$ by the circular beam cross-sections, the dimensionless boundary value problem is

$$F[y] = \{m^2y''\}'' + py'' + \lambda^2 my = 0,$$

$$y = 0 \quad \text{and} \quad y' = 0 \ \text{at} \ x = 0,$$

$$m^2y'' + \tfrac{4}{3}\lambda^2\zeta^2\kappa^4(y + \tfrac{7}{5}\zeta\kappa y') = 0 \ \text{and}$$

$$\{m^2y''\}' - \tfrac{4}{3}\lambda^2\zeta\kappa^3(y + \zeta\kappa y') = 0 \quad \text{at} \ x = 1. \tag{10}$$

The overbars have been dropped for the sake of simple notation and in the following, all variables will be referred to in their dimensionless form. It is noted that the dimensionless mass ratio

$$\mu = \frac{\text{mass of rocket motor}}{\text{mass of column}} = \frac{M}{m_0 L}$$

and the dimensionless end-ball (rocket motor) rotatory inertia

$$\upsilon = \frac{\text{rotatory inertia of the rocket motor about its centroid}}{3 \times (\text{rotatory inertia of the column about its end})} = \frac{J}{m_0 L^3}$$

defined in [1], are given by

$$\mu = \tfrac{4}{3}\zeta\kappa^3, \qquad \upsilon = \tfrac{2}{5}\zeta^2\kappa^2\mu = \tfrac{8}{15}\zeta^3\kappa^5 \tag{11}$$

in terms of the variables ζ and κ.

Contrary to a damped column, the equilibrium configuration $y(x) \equiv 0$ is only marginally stable by sufficiently small load values as the real parts of all eigenvalues

are equal to zero. Flutter is initiated when two eigenvalues and their corresponding eigenvectors coalesce, since one of the eigenvalues gets a positive real part beyond this point. Divergence cannot occur in the present system [3].

2.2. THE ADJOINT SYSTEM

In connection with the optimization, consideration of the adjoint system to equation (10) is necessary. It is determined by solving the equation

$$\int_0^1 vF[y]\,\mathrm{d}x - \int_0^1 yF^*[v]\,\mathrm{d}x = 0 \tag{12}$$

which gives

$$F^*[v] = \{m^2v''\}'' + pv'' + \lambda^2 mv = 0,$$

$$v = 0 \text{ and } v' = 0 \text{ at } x = 0,$$

$$m^2v'' + pv + \tfrac{4}{3}\lambda^2\zeta^2\kappa^4(v + \tfrac{7}{5}\zeta\kappa v') = 0 \text{ and}$$

$$\{m^2v''\}' + pv' - \tfrac{4}{3}\lambda^2\xi\kappa^3(v + \zeta\kappa v') = 0 \quad \text{at } x = 1. \tag{13}$$

This boundary value problem describes small oscillations of a column being compressed by a force with a fixed line of action coinciding with the axis x and also having the finite size end-mass. The system is shown in Figure 3. The case where the end-mass is a point-mass is treated in Bolotin's book [3]. The force can be realized by an air-jet impinging on a rigid, 'massless' (in reality, very stiff and light-weighted) end-plate [19, 20].

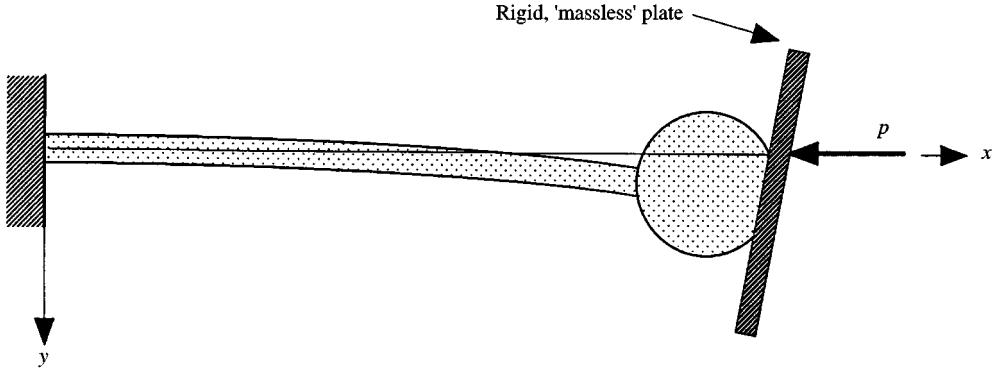

Figure 3. Sketch of the adjoint system.

2.3. DISCRETIZATION

When the column is uniform, eigensolutions (λ, y) can be obtained 'exactly', without discretization [1]. This is not possible for a column with non-linear tapering. In the following the finite element method is applied [21]. Within each element, the deflection function $y(x)$ is represented by polynomials. The discretized version of equation (10) takes the form

$$\mathbf{Fd} = [\lambda^2\mathbf{M}(\mathbf{m}, \zeta, \kappa) + \mathbf{S}(\mathbf{m}) - p(\mathbf{Q}_C - \mathbf{Q}_N)]\mathbf{d} = \mathbf{0}. \tag{14}$$

The vector $\mathbf{m} = \{m_1, m_2, \ldots, m_{Ne+1}\}$ represents the design variables which are the specific masses $m(x)$ at the $N_e + 1$ nodal points. Thus, $m_1 = m(0)$ and $m_{Ne+1} = m(1)$. The mass distribution is assumed to vary linearly within each element. The mass matrix is represented by $\mathbf{M}$, $\mathbf{S}$ is the stiffness matrix, $\mathbf{Q}_C$ is the conservative load matrix and $\mathbf{Q}_N$ is the non-conservative load matrix. Finally, $\mathbf{d}$ is the nodal displacement vector. The matrices $\mathbf{M}$, $\mathbf{S}$ and $\mathbf{Q}_C$ are symmetric and positive definite, while $\mathbf{Q}_N$ is non-symmetric. The discretized version of the adjoint system (13) is

$$\mathbf{F}^T\mathbf{b} = \mathbf{0}. \tag{15}$$

The flutter condition is [22]

$$\mathbf{b}^T\mathbf{Md} = 0. \tag{16}$$

The numerical results to follow were obtained with the column divided into 20 elements of the same length. The matrix system (14) is thus of size 40×40. The eigenvalues λ (identical for (15) and (16)) were determined by using the QR-algorithm [23]. The critical load p_{cr} was determined by using a bisection method. Equation (16) was used to check the accuracy.

3. FLUTTER OSCILLATIONS OF THE UNIFORM COLUMN

3.1. THE FLUTTER LIMIT

The influence of the size of the end-ball on the stability limit of a uniform column will briefly be considered first. Figure 4(a) shows the stability map, depicting ρ_{cr} as function of $n = a/r_0$ for various values of the columns slenderness ratio $\zeta = r_0/L$. Figure 4(b) illustrates the depenence of the flutter frequency on the ratios ζ and κ. It will be seen that increasing κ results in decreasing flutter frequency and it decreases most rapidly when ζ is large.

3.2. THE FLUTTER VIBRATIONS

Figure 5 illustrates how the size of the end-ball affects the flutter oscillations of the column. Here, and in all the following numerical examples, only the slenderness

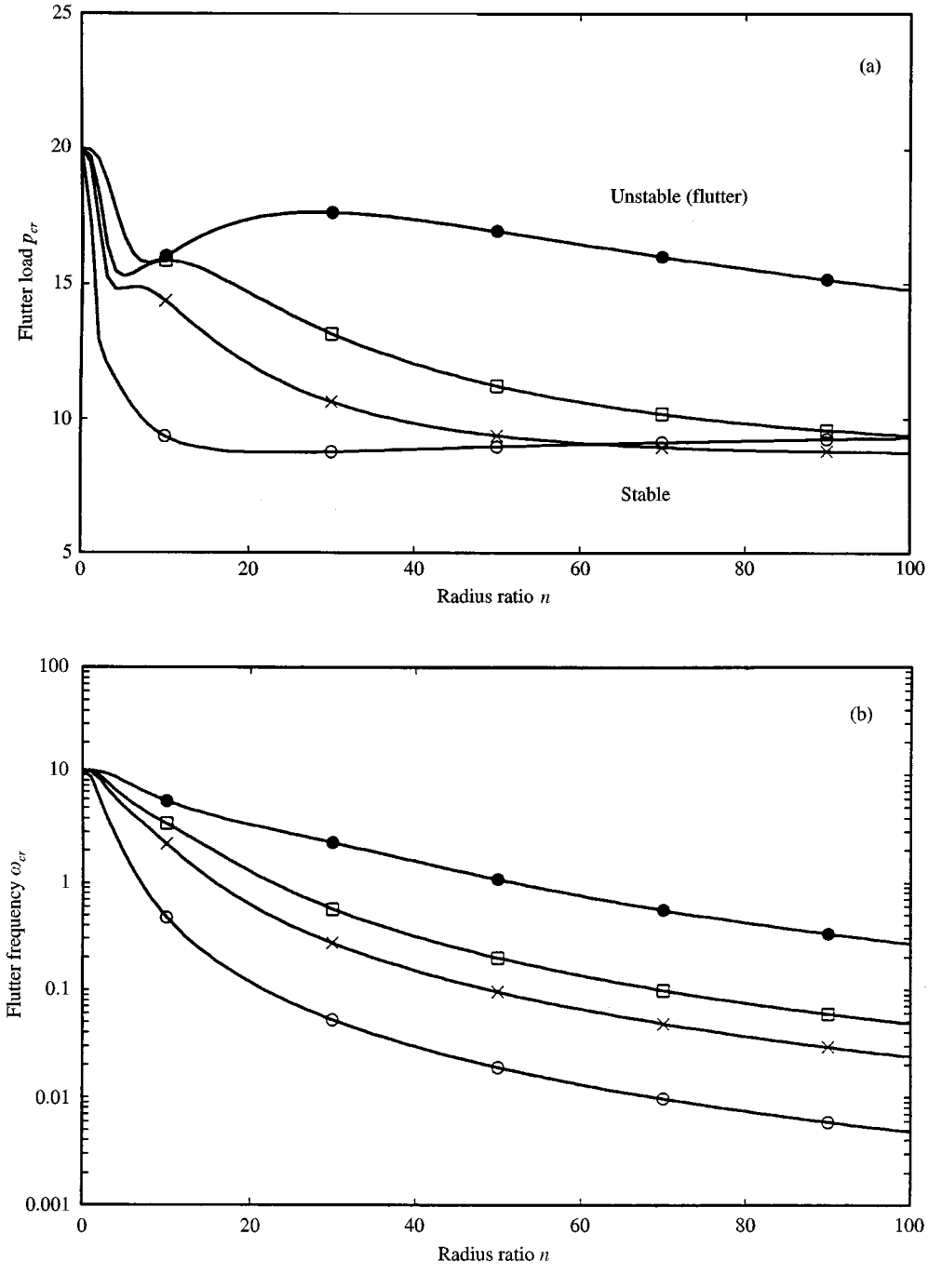

Figure 4. (a) Stability limits as functions of the radius ratio $\kappa = a/r_0$ for various values of the slenderness ratio $\zeta = r_0/L$; (b) The corresponding flutter frequencies. —●— = 0·001, —□— = 0·05, —×— = 0·01, —○— = 0·05

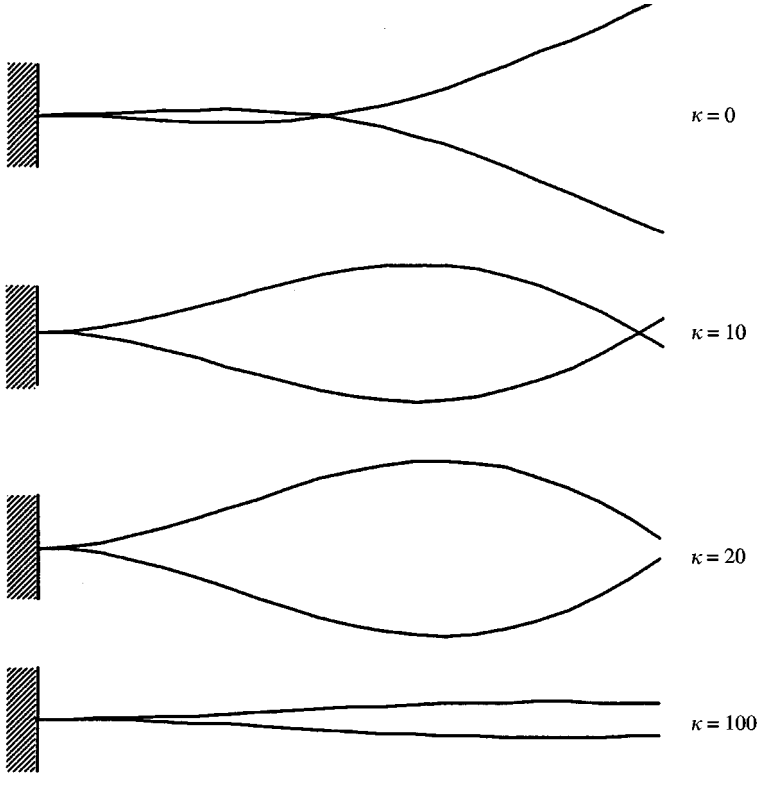

Figure 5. Flutter oscillations for various values of the radius ratio κ (slenderness ratio $\zeta = 0{\cdot}01$).

ratio $\zeta = r_0/L = 0{\cdot}01$ will be considered. It will be seen that the nodal point moves towards the free end by increasing κ and by a certain κ-value, it disappears. For a uniform column, flutter is always initiated by coincidence of the first and the second eigenvalue branch, so it means that the nodal point of the second eigenmode disappears by a certain κ-value. What qualitatively differentiates the second eigenmode from the first then, is that the bending moment for the second eigenmode vanishes at an inner point, $0 < x < 1$.

4. OPTIMIZATION

4.1. PROBLEM FORMULATION

Let $p_1, p_2, \ldots, p_{Ne}$ be the loads at which pairs of eigensolutions coincide and let p_{cr} be the smallest of these values. For the uniform column, it is assumed that $p_1 < p_2 < \cdots < p_{Ne}$. The optimization problem is to determine the design vector $\mathbf{m}$ which

$$\text{Maximize } p_{cr} \tag{17}$$

subject to

(i) $p_{cr} \leqslant \{p_1, p_2, \ldots, p_{N_e}\}$,

(ii) $\omega_{n+1} - \omega_n < \begin{cases} 0 & \text{for } n = 1, 3, 5, \ldots \\ c_+ & \text{for } n = 2, 4, 6, \ldots \end{cases}$ for all $p < p_{cr}$,

(iii) $\underline{m}_j \leqslant m_j \leqslant \bar{m}_j, \quad j = 1, 2, \ldots, N_e + 1,$

(iv) Volume = constant.

Here, $\omega_n = \omega_n(p)$ denotes the *load-frequency curves* which are the imaginary parts of the eigenvalue brances $\lambda_n(p)$. For $p = 0$, $\omega_1 < \omega_2 < \cdots < \omega_{Ne}$. The constraints (17-ii) make sure that the 'nature' of these curves remains unchanged; ω_1 and ω_2 coincide at the load p_1, ω_3 and ω_4 at the load p_2, and so on. Coincidence between, for example, ω_2 and ω_3 is thus prevented. These curves are kept apart by a specified distance c_+. This is done in order to increase the 'robustness' of the optimal columns. The optimal flutter load p_{cr} may be made slightly larger by setting $c_+ = 0$, but a small change in the design variables may then cause a big drop in p_{cr}, as discussed in reference [13].

4.2. SOLUTION METHOD

The non-linear optimization problem (17) is linearized and solved iteratively by using sequential linear optimization (linear programming). After k iterations the design is specified by the vector $\mathbf{m}^k$. The $(k+1)$th optimal redesign problem (for determining the design vector $\mathbf{m}^{k+1} = \mathbf{m}^k + \Delta\mathbf{m}$) can be written as

$$\text{Maximize } p_{cr}$$

$$\textit{subject to} \tag{18}$$

(i) $p_{cr} \leqslant p_l^{k+1} \approx p_l^k + \sum_{j=1}^{N_e+1} \frac{\partial p_l^k}{\partial m_j} \Delta m_j, \quad l = 1, 2, \ldots, N_e,$

(ii) $\omega_{n+1}^{k+1} - \omega_n^{k+1} \approx \omega_{n+1}^k - \omega_n^k + \sum_{j=1}^{N_e+1} \frac{\partial(\omega_{n+1}^k - \omega_n^k)}{\partial m_j} \Delta m_j \leqslant \begin{cases} 0 & \text{for } n = 1, 3, 5, \ldots, \\ c_+ & \text{for } n = 2, 4, 6, \ldots. \end{cases}$

for $p = p_1^*, p_2^*, \ldots, p_{cr}$,

(iii) $\underline{m}_j \leqslant m_j^k + \Delta m_j \leqslant \bar{m}_j, \quad j = 1, 2, \ldots, N_e + 1,$

(iv) $\mathbf{l}^T \Delta\mathbf{m} = 0.$

Here, $\mathbf{l}$ is a vector of the elements which are linear combinations of the element lengths l_e,

$$\mathbf{l} = \tfrac{1}{2}\{l_1, l_1 + l_2, l_2 + l_3, \ldots, l_{Ne-1} + l_{Ne}, l_{Ne}\}. \tag{19}$$

The discrete load values $p_1^*, p_2^*, \ldots$, are in the range between 0 and p_{cr}. The derivatives of p_{cr} and ω with respect to the design parameters m_j, $j = 1, 2, \ldots, N_e + 1$, are given by [13, 24]

$$\frac{\partial p_{cr}}{\partial m_j} = \frac{\mathbf{b}^T[\partial \mathbf{F}/\partial m_j]\mathbf{d}}{\mathbf{b}(\mathbf{Q}_C - \mathbf{Q}_N)\mathbf{d}}, \qquad \frac{\partial \omega}{\partial m_j} = \frac{\mathbf{b}^T[\partial \mathbf{F}/\partial m_j]\mathbf{d}}{2\omega \mathbf{b}^T \mathbf{M}\mathbf{d}}. \tag{20}$$

The eigenvectors $\mathbf{d}$ and $\mathbf{b}$ can be obtained from (14) and (15). The sizes of the design changes are governed by the limits $\Delta m_j^{\min}$, $\Delta m_j^{\max}$, $j = 1, 2, \ldots, N_e + 1$, such that

$$0 \geqslant \Delta m_j^{\min} \leqslant \Delta m_j \leqslant \Delta m_j^{\max} \geqslant 0. \tag{21}$$

Linearized system (18) can be converted into a pure linear programming problem by defining the positive variables

$$\Delta m_j^+ = \Delta m_j - \Delta m_j^{\min} \geqslant 0. \tag{22}$$

In terms of these variables, the design change limits are given by

$$\Delta m_j^+ \leqslant \Delta m_j^{\max} - \Delta m_j^{\min}. \tag{23}$$

The sequence of linear programming problems (18) are solved (for $k = 1, 2, \ldots$) by using the Simplex method [23]. In the numerical results to follow, the eigenvalue margin c_+ in (18-ii) was set to $c_+ = 15$. The number of load values p_j^* at which these constraints were evaluated was 40. The sequence of iterations was terminated when the increase in the critical load between two successive iterations became less than 10^{-4}. Uniform columns were taken as initial designs.

5. NUMERICAL RESULTS

Figure 6 shows the optimal columns for various values of the radius ratio κ in the range from $\kappa = 0$ to $\kappa = 100$. The functions $\pm\sqrt{m(x)}$ are shown in an appropriate scaling, approximated by the nodal values $\pm\sqrt{m_j}$ connected with straight lines. The flutter oscillations are shown as well. The considered range of κ gives a rather full picture of how the size of an end-mounted rocket motor affects the optimum design of the column, as the dimensionless mass ratio μ and the dimensionless end-mass (rocket motor) rotatory inertia υ, given in (11), vary from $\mu = 0$, $\upsilon = 0$, to $\mu > 10^4$, $\upsilon > 5 \times 10^3$. The results are summarized in Table 1. Table 2 gives the design parameters m_j for the optimal columns shown in Figure 6.

Figure 6(a) shows the optimal Beck's column which is the 'limit case' of vanishing end-mass ($\kappa = 0$). A very large increase of the flutter load p_{cr} is possible; about eight times. It should be noted that this design was obtained by solving the dual problem of equation (18), namely: minimize the volume of the column under the constraint of a constant flutter load. The obtained minimum-volume design was then scaled

up to unit volume [16]. This method seems to avoid some local optima where the algorithm based on equation (18) tends to stop. An increase in p_{cr} of about five time seems to be the 'record' when a formulation similar to equation (18) is used, see reference [25]. The 'inversion' of the problem is however not legitimate when the end-ball is present. Figure 7(a) shows the load-frequency curves for the optimal Beck's column. Flutter is initiated by simultaneous coincidence of the frequency couples (ω_1, ω_2) and $(\omega_{11}, \omega_{12})$. The couple (ω_3, ω_4) coincide at an only slightly larger load value. The flutter vibrations thus occur under more interacting frequencies. This is analogous to the multiple-modal buckling of the optimally designed clamped–clamped column [26].

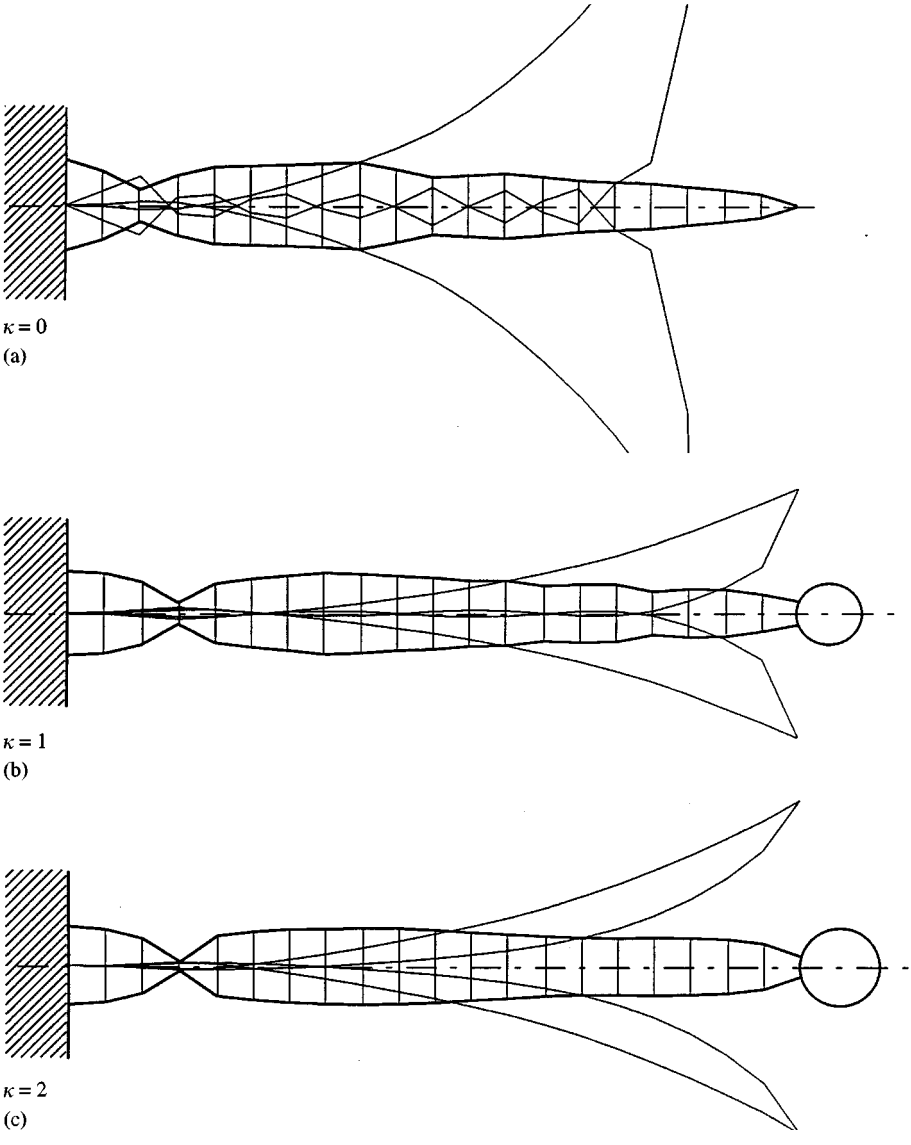

Figure 6. Optimal columns and their flutter modes for various values of κ ($\zeta = 0{\cdot}01$).

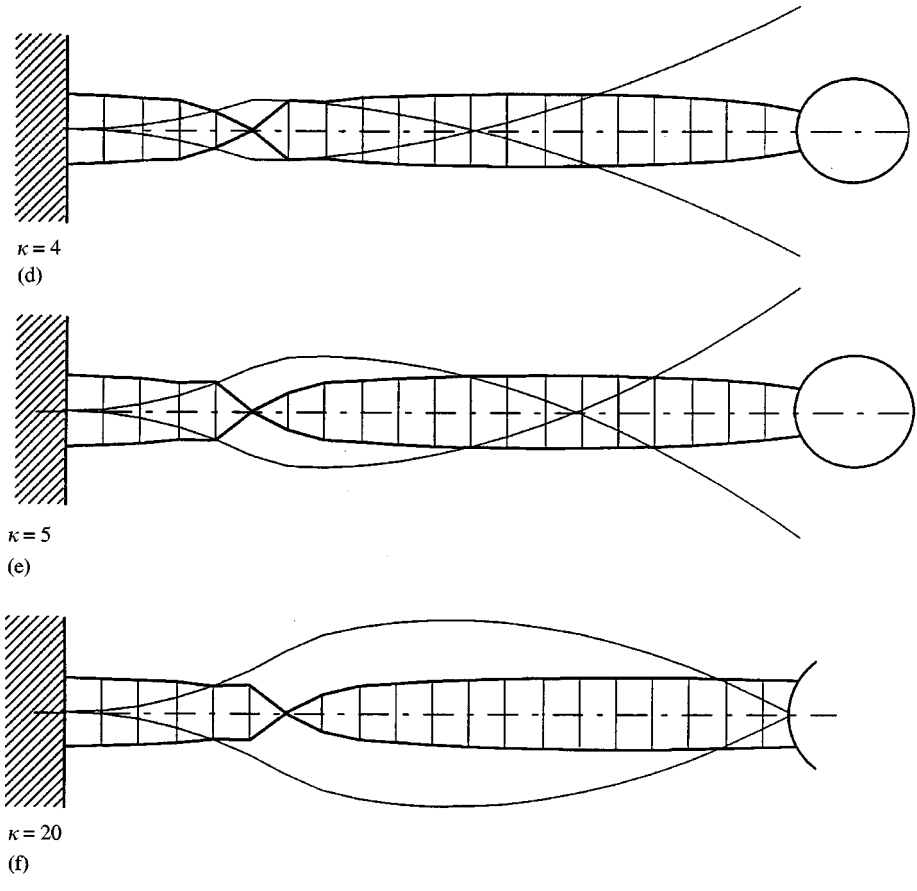

Figure 6. (*Continued*).

Figure 6(b) shows the optimal design with a relatively small end-ball ($\kappa = 1$). The critical load p_{cr} is increased about 4·5 times. The eigenvalue branch distance $c_+ = 15$ turned out to be too big in this case as the fourth and the fifth branch (ω_4 and ω_5) tended to coincide and consequently 'locked' the optimization by $p_{cr} \approx 60$. Consequently, c_+ was decreased to 5. The load–frequency curves are shown in Figure 7(b). Due to the relatively small value of c_+, the seventh and the eighth branch (ω_7 and ω_8) coincide at the critical load, simultaneously with coincidence between the first and the second one. The third and the fourth branch coincide at a just slightly higher load.

Figure 6(c) shows the optimal design for $\kappa = 2$. Here the critical load is increased about three times. This column has also two pairs of coinciding eigenvalue branches at the flutter load, as shown in Figure 7(c). It should be noted that the critical load probably may be raised slightly more by decreasing the parameter $c_+ (c_+ = 15$ is used) but as no 'troublesome' eigenvalue branch interactions occur, no major changes are expected.

For $\kappa \geqslant 4$, a 'joint' develops as one design variable reaches the lower limit $\underline{m}_j = 10^{-8}$, see Figure 6(*d–j*). An optimum is reached by just one pair of coinciding

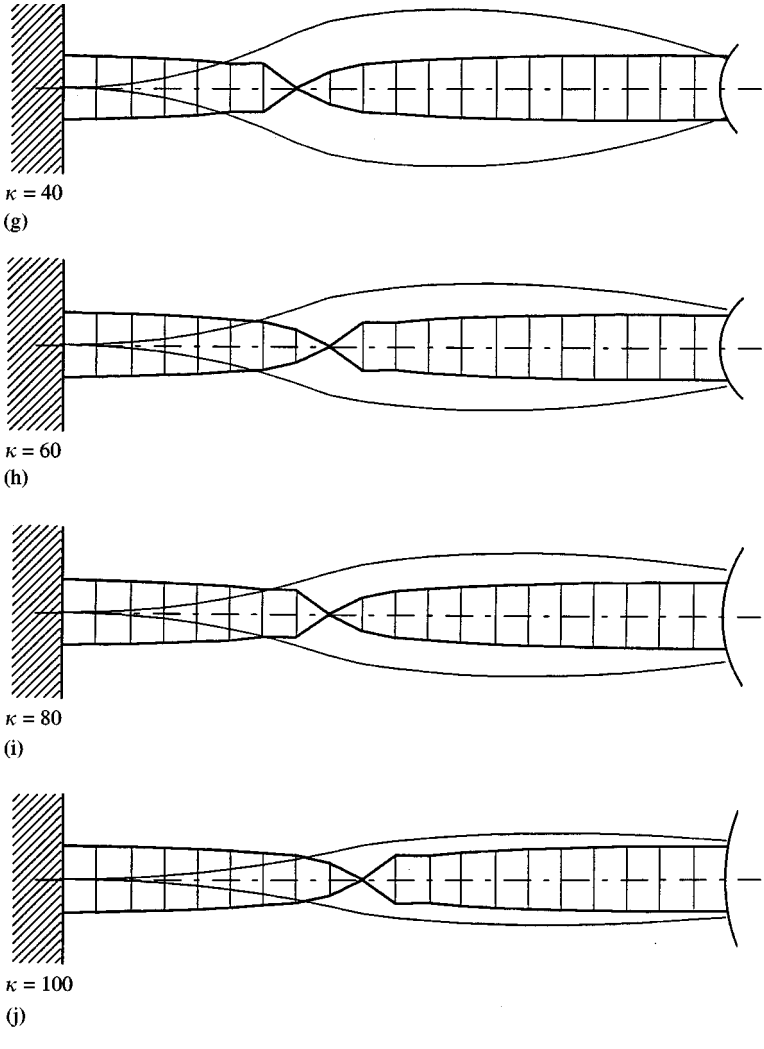

Figure 6. (*Continued*).

eigenvalue branches and the lower limit $\underline{m}_j$ is reached at the nodal point where the (single) bending moment function changes sign. It should be stressed that it is not a link; the mass and stiffness are not zero, but small. The first eigenfrequency of the columns is thus not zero. Figure 7(d) shows the load–frequency curves for $\kappa = 5$. These curves are qualitatively similar for $\kappa = 4$ and for $\kappa > 5$. As an optimum is reached by just one pair of coinciding eigenvalue branches, the gradient expression

$$g_j = \frac{\partial p_{cr}}{\partial m_j} \frac{1}{l_{j-1} + l_j} = \text{same positive constant}, \quad (l_0 = l_{Ne+1} = 0) \tag{24}$$

for all node numbers $j = 1, 2, \ldots, N_e + 1$, except for the node(s) where $m_j = \underline{m}_j$. Here the gradient expression has a lower value. This implies that p_{cr} has reached an,

TABLE 1
Summary of results obtained for $\zeta = 0{\cdot}01$

$\kappa = a/r_0$	$\mu = M/m_0L$ $= 4\zeta\kappa^3/3$	$v = J/(m_0L^3)$ $= 8\zeta^3\kappa^5/15$	p_{cr}^{uni} for the uniform column	p_{cr}^{opt} for the optimal column	Gain factor $p_{cr}^{opt}/p_{cr}^{uni}$
0	0	0	20·05	159·35	7·95
1	0·013333	$5{\cdot}3333 \times 10^{-7}$	19·51	87·38	4·48
2	0·10667	$1{\cdot}7067 \times 10^{-5}$	17·08	55·15	3·23
4	0·85333	$5{\cdot}4613 \times 10^{-4}$	14·81	20·64	1·39
5	1·6667	$1{\cdot}6667 \times 10^{-3}$	14·84	19·83	1·34
20	106·67	1·7067	12·01	15·80	1·32
40	853·33	54·613	9·84	13·39	1·36
60	2880·0	414·72	9·11	12·50	1·37
80	6826·7	1747·6	8·84	12·14	1·37
100	13333·0	5333·3	8·75	11·95	1·37

TABLE 2
Mass parameters m_j *for the optimal columns obtained for* $\zeta = 0{\cdot}01$ with 20 finite elements and $\underline{m}_j = 10^{-8}$

e	$\kappa = 0$	$\kappa = 1$	$\kappa = 2$	$\kappa = 4$	$\kappa = 5$	$\kappa = 20$	$\kappa = 40$	$\kappa = 60$	$\kappa = 80$	$\kappa = 100$
1	2·1433	1·7913	1·5639	1·2712	1·2838	1·2075	1·2852	1·3144	1·3344	1·3874
2	1·2100	1·6310	1·3356	1·1684	1·1783	1·1448	1·2284	1·2640	1·2886	1·3458
3	0·2773	1·0203	0·7575	0·9859	1·0707	1·0505	1·1528	1·1961	1·2259	1·2881
4	0·9237	0·1212	0·02084	0·8922	0·8195	0·9523	1·0484	1·1057	1·1451	1·2122
5	1·5550	0·9002	0·9296	0·3429	0·8769	0·7278	0·9404	0·9992	1·0363	1·1186
6	1·6307	1·1999	1·1945	10^{-8}	10^{-8}	0·7674	0·7166	0·8415	0·9250	1·0041
7	1·7135	1·4167	1·3695	0·9066	0·3607	10^{-8}	0·7333	0·7102	0·7035	0·8454
8	1·8252	1·6986	1·4562	0·8226	0·8372	0·3627	10^{-8}	0·3304	0·7061	0·7025
9	1·9432	1·5989	1·4950	1·0683	0·9485	0·7403	0·3428	10^{-8}	10^{-8}	0·3341
10	1·4019	1·4287	1·4627	1·1658	1·1103	0·8796	0·7154	0·7295	0·3464	10^{-8}
11	0·8703	1·3186	1·3403	1·2604	1·2054	1·0321	0·8462	0·7000	0·6948	0·7256
12	0·9744	1·0998	1·1761	1·3168	1·2774	1·1343	0·9963	0·9214	0·8328	0·6889
13	1·0878	1·0762	1·0480	1·3490	1·3192	1·2143	1·0991	1·0268	0·9818	0·9086
14	0·8864	0·7979	0·9202	1·3541	1·3355	1·2684	1·1829	1·1295	1·0876	1·0122
15	0·6862	0·8698	0·8405	1·3332	1·3256	1·3018	1·2428	1·2041	1·1738	1·1144
16	0·6122	0·8395	0·8174	1·2833	1·2889	1·3144	1·2855	1·2603	1·2409	1·1886
17	0·5349	0·4921	0·8559	1·2022	1·2229	1·3072	1·3092	1·3008	1·2877	1·2462
18	0·3914	0·6100	0·8298	1·0848	1·1246	1·2791	1·3149	1·3217	1·3202	1·2866
19	0·2608	0·5607	0·7632	0·9234	0·9869	1·2304	1·3054	1·3301	1·3365	1·3094
20	0·1404	0·3587	0·5528	0·7087	0·8014	1·1540	1·2734	1·3179	1·3375	1·3187
21	10^{-8}	0·1310	0·1052	0·3917	0·5398	1·0684	1·2465	1·2980	1·3236	1·3121

at least, local optimum. This is proved in the Appendix 1. Figure 8 shows the gradient function (24) for $\kappa = 5$, for both the uniform and the optimal column. In terms of the gradient function, the occurrence of a 'joint' is explained by the fact that the critical load increases more by adding material at any other location than

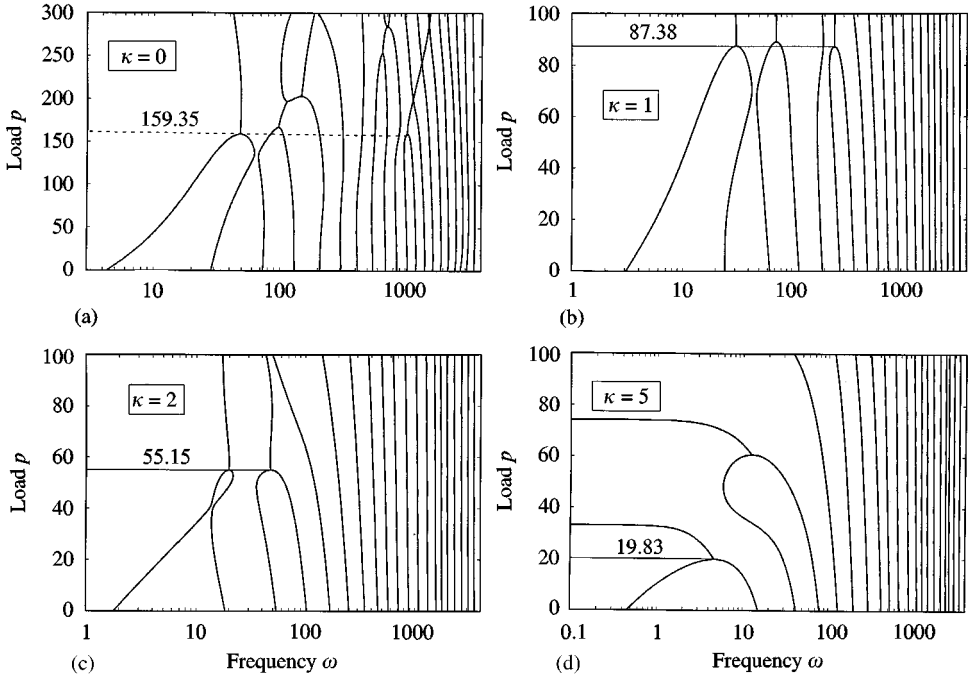

Figure 7. Load–frequency curves for some of the optimal columns. (a) $\kappa = 0$; (b) $\kappa = 1$; (c) $\kappa = 2$; (d) $\kappa = 5$.

at the joint. In fact, since $\partial p_{cr}/\partial m_6 < 0$ the gradient function shows that the critical load *decreases* by adding material at the joint, even if the volume is increased.

The 'jointed' optimal columns shown in Figure 6 may not be very useful in practical applications and should be considered as the limited solutions of the optimal design problem. More practical columns are obtained by increasing the minimum allowable cross-section area. Figure 9(a) shows the optimum design for $\kappa = 5$, obtained with the lower limit $\underline{m}_j = 0{\cdot}25$ for all design variables. This means that the minimum allowable diameter $d_{\min} = \sqrt{(0{\cdot}25)}d_0 = 0{\cdot}5d_0$, that is, half of the diameter of the uniform start-design column. The critical load is $p_{cr} = 19{\cdot}38$, as opposed to $p_{cr} = 19{\cdot}83$ for $\underline{m}_j = 10^{-8}$. *Practical columns can thus be obtained with just a minor drop of the gain factor* $p_{cr}^{opt}/p_{cr}^{uni}$. In Figure 9(b) the lower limit $m_j = 0{\cdot}5$, giving $d_{\min} = 0{\cdot}707d_0$. The critical load is $p_{cr} = 18{\cdot}85$.

To see how the optimum design is affected by the number of design variables, the case $\kappa = 5$ was recalculated using 40 finite elements and 41 design variables. Figure 10 shows the result. The critical load is 20·38, which is 2·8% larger than the load obtained with 20 elements and 21 design variables. The joint is located at the same position, $x = 0{\cdot}25$.

The optimum solutions change very little by increasing κ from the value $\kappa = 4$. It appears that the flutter frequency in any case is so low that the elastic restoring forces by far dominates over the inertia forces of the column and are in dynamic balance with the inertia forces of the end-ball. [It is noted that the flutter frequencies change very little by optimization. The frequencies for the uniform

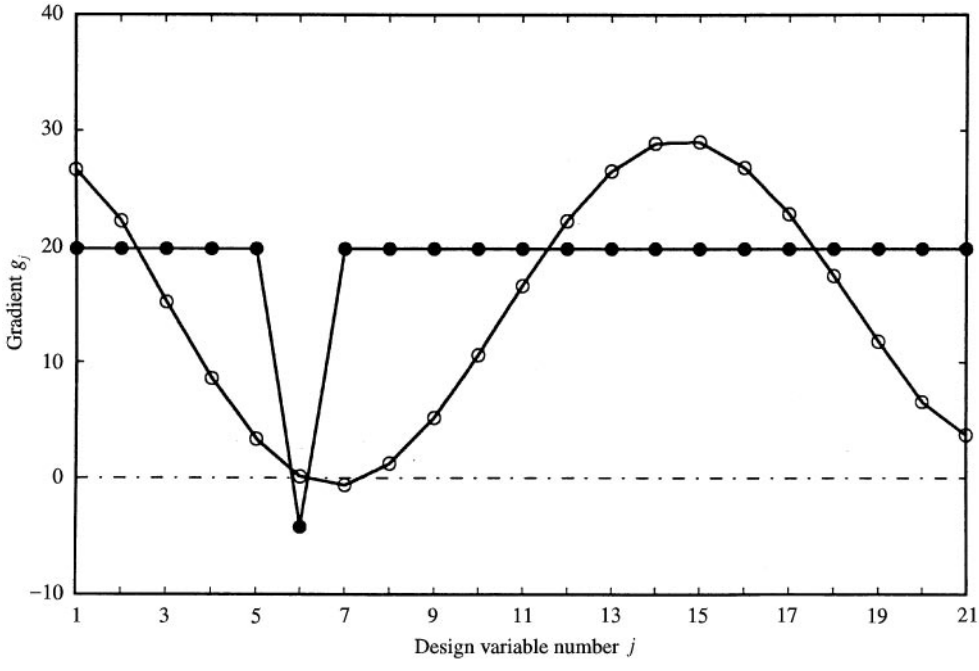

Figure 8. The gradient expression (27) evaluated for the uniform and the optimal columns by $\kappa = 5$. —●— Optimal, —⊖— Uniform

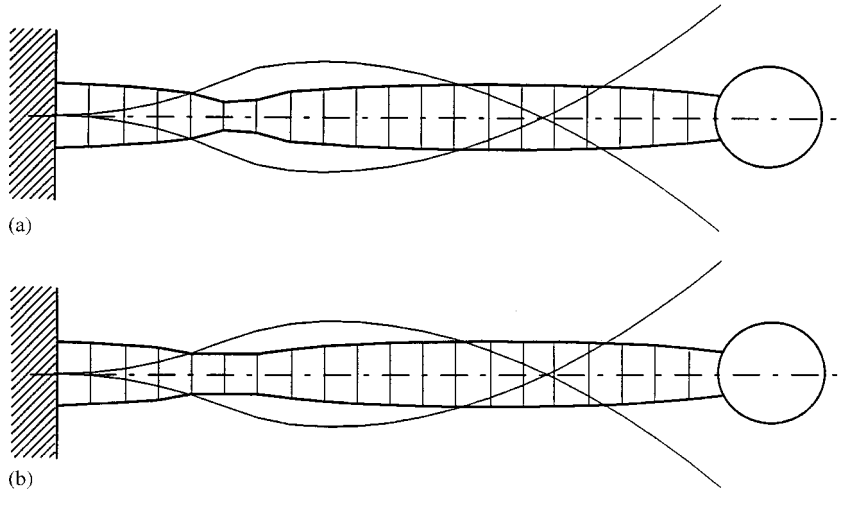

Figure 9. Optimal columns for $\kappa = 5$ with increased constraints on the minimum thickness. (a) $\underline{m}_j = 0{\cdot}25$: $p_{cr} = 19{\cdot}38$; (b) $\underline{m}_j = 0{\cdot}50$: $p_{cr} = 18{\cdot}85$.

columns are shown in Figure 4(b).] The gain factor $p_{cr}^{opt}/p_{cr}^{uni}$ is only 1·3–1·4 which is similar to what can be obtained by a pure conservative loading [17]. The gain factor does not change much by continued increase in κ. It is noted that the neglect of shear deformation may be questionable for, say, $\kappa > 4$. The purpose of,

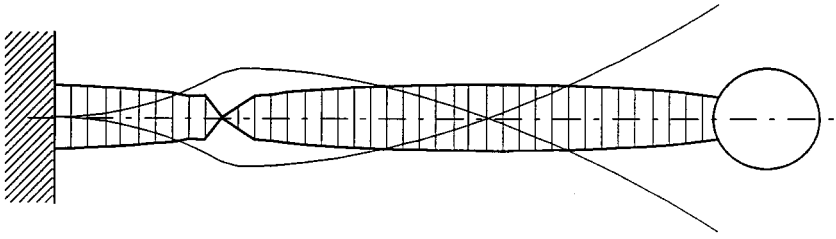

Figure 10. The optimal column for $\kappa = 5$ using 40 finite elements and 41 design variables. The flutter load is $p_{cr} = 20{\cdot}38$.

nevertheless, to consider larger values of κ is to get an overview of how the size of the end-ball affects the optimum design of the simplest beam model. This model gives the first order approximation to the solution of the problem. Further studies could take rotatory inertia and shear deformation of the column into consideration. In particular, this may eliminate the formation of a joint. Due to the low flutter frequencies, the rotatory inertia of the columns is not expected to be significant.

6. CONCLUSIONS

The strongest columns with respect to dynamic instability (flutter), caused by the thrust of an end-mounted rocket motor, have been calculated for various motor sizes. The motor was simplified as a massive ball with same material density as the column. The main conclusions are as follows.

(1) For small ball-sizes, the critical thrust can be increased significantly. Dynamic instability occurs by two or three interacting frequencies. By increasing the ball-size, the gain of optimization is significantly reduced.
(2) By the mass-ratios which can be realized experimentally, $\mu =$ (mass of rocket motor)/(mass of column) > 1, the critical thrust can only be increased by a factor 1·3–1·4. This is similar to what can be obtained in the case of a pure conservative end-loading. Dynamic instability occurs by a single flutter frequency. It has been shown that the optimal columns then satisfy a simple optimality criteria.
(3) The great sensitivity to small changes in design parameters and the optimization method dependency of Beck's problem are not present for 'practical' values of the mass-ratio μ.

ACKNOWLEDGMENTS

Financial support for this investigation is due to the Japan Society for the Promotion of Science (JSPS). The first author (ML) would like to express his deep gratitude to JSPS for the postdoctoral fellowship (fiscal years 1996, 1997) to conduct research in Japan. The support from the Danish Research Academy and from Prof. Pauli Pedersen at the Technical University of Denmark is also gratefully acknowledged.

REFERENCES

1. Y. Sugiyama, K. Katayama and S. Kinoi 1995 *Journal of Aerospace Engineering* **8**, 9–15. Flutter of cantilevered column under rocket thrust.
2. Y. Sugiyama, J. Matsuike, B.-J. Ryu, K. Katayama, S. Kinoi and N. Enomoto 1995 *AIAA Journal* 33(3), 499–503. Effect of concentrated mass on stability of cantilevers under rocket thrust.
3. V. V. Bolotin 1963 *Nonconservatie Problems of the Theory of Elastic Stability*. Oxford: Pergamon Press.
4. H. Leipholz 1980 *Stability of elastic systems*. Alphen ann den Rijn: Sijthoff & Noordhoff.
5. W. T. Koiter 1996 *Journal of Sound and Vibration* **194**, 636–638. Unrealistic follower forces.
6. Y. Sugiyama, M. A. Langthjem and B.-J. Ryu 1999 *Journal of Sound and Vibration* **224**, 779–782. Realistic follower forces.
7. G. Hermann 1971 *NASA Contractor Report CR*-1782. Dynamics and stability of mechanical systems with follower forces.
8. G. Hermann and I.-C. Jong 1965 *Journal of Applied Mechanics* **33**, 592–597. On the destabilizing effect of damping in nonconservatice elastic systems.
9. A. P. Seyranian 1990 *Advances in Mechanics* **13**, 89–124. Destabilizing paradox in stability problems of nonconservative systems.
10. M. A. Langthjem 1996 *Ph.D. Thesis, Department of Solid Mechanics, Technical University of Denmark*. Dynamics, stability and optimal design of structures with fluid interaction.
11. F. Odeh and I. Tadjbakhsh 1975 *Journal of Optimization Theory and Applications* **15**, 103–118. The shape of the strongest column with a follower load.
12. J. L. Claudon 1975 *Journal de Mechanique* **14**, 531–543. Characteristic curves and optimum design of two structures subjected to circulatory loads.
13. M. Hanaoka and K. Washizu 1980 *Computers and Structures* **11**, 473–480. Optimum design of Beck's column.
14. Y. Seguchi, Y. Tada and K. Kema 1984 *Proceedings of the JSME Series A*, 679–686. Shape decision of nonconservatie structural systems by the inverse variable principle.
15. U. T. Ringertz. 1994 *Structural Optimization* **8**, 120–124. On the design of Beck's column.
16. M. Langthjem and Y. Sugiyama 1999 *Computers and Structures*. Optimum design of cantilevered columns under the combined action of conservative and nonconservative loads. I. The undamped case. II. The damped case [to appear].
17. A. Gajewski and M. Zykowski 1988 *Optimal Structural Design under Stability Constraints*. Dortrecht: Kluwer.
18. B.-J. Ryu and Y. Sugiyama 1994 *Computers and Structures* **51**, 331–335. Dynamic stability of cantilevered Timoshenko columns subjected to a rocket thrust.
19. W. T. Feldt, S. Nemat-Nasser, S. N. Prasad and G. Herrmann 1969 *Journal of Applied Mechanics* **36**, 693–701. Instability of a mechanical system induced by an impinging air jet.
20. Y. Sugiyama, T. Katayama and B.-J. Ryu 1992 *Proceedings of the Dynamics and Design Conference, Hokkaido, Japan*. Vibration and stability of columns under nonconservative forces realized by an impinging jet.
21. R. D. Cook, D. S. Malkus and M. E. Plesha 1989 *Concepts and applications of finite element analysis*. New York: Wiley.
22. R. H. Plaut 1972 *AIAA Journal* **10**, 967–968. Determining the nature of instability in nonconservative problems.
23. W. H. Press, S. A. Teukolsky, V. T. Vetterling and B. P. Flannery 1992 *Numerical Recipes in Fortran*, Cambridge: Cambridge University Press; [second edition].
24. P. Pedersen and A. P. Seyranian 1983 *International Journal of Solids and Structures* **19**, 315–335. Sensitivity analysis for problems of dynamic stability.

25. R. ISHIDA and Y. SUGIYAMA 1997 *Transactions of the Japan Society of Mechanical Engineers* **63**, 195–200. On the optimal shape of a column subjected to a follower force.
26. N. OLHOFF and S. H. RASMUSSEN 1977 *International Journal of Solids and Structures* **13**, 605–614. On single and bimodal optimum buckling loads of clamped columns.

APPENDIX 1: OPTIMALITY BY A SINGLE FLUTTER LOAD (WITH ONE UNIQUE FLUTTER FREQUENCY)

Finite element number e has length l_e, volume V_e, and left- and right-side cross-section areas m_e/ρ and m_{e+1}/ρ respectively. The total column-volume V is given by

$$V = \sum_{e=1}^{Ne} V_e = \frac{1}{2\rho} \sum_{e=1}^{Ne} l_e[m_e + m_{e+1}] = \frac{1}{2\rho} \sum_{e=1}^{Ne+1} m_e[l_{e-1} + l_e],$$

$$\text{with } l_0 = l_{Ne+1} = 0. \tag{A1}$$

Assume that the design parameters $m_{c1}, m_{c2}, \ldots, m_{cN}$ have reached their lower limits $\underline{m}_i$. The increment in the critical load due to variations in the design parameters is given by

$$\delta p_{cr} = \sum_{e=1}^{Ne+1} \frac{\partial p_{cr}}{\partial m_e} \delta m_e = 2\rho \sum_{e=1}^{Ne+1} \frac{\partial p_{cr}}{\partial m_e} \frac{1}{l_{e-1} + l_e} \underbrace{\frac{1}{2\rho} \delta m_e[l_{e-1} + l_e]}_{\delta V} \tag{A2}$$

For load maximization by constant volume, $\delta V = 0$. From (A2) it will be seen that if

$$\frac{\partial p_{cr}}{\partial m_e} \cdot \frac{1}{l_{e-1} + l_e}\bigg|_{\substack{e=1,2,\ldots,N_e+1 \\ e \neq c1,c2,\ldots,cN}} = \text{same positive constant '}k_1\text{'} > \frac{\partial p_{cr}}{\partial m_e} \cdot \frac{1}{l_{e-1} + l_e}\bigg|_{e=c1,c2,\ldots,cN} \tag{A3}$$

with $l_0 = l_{Ne+1} = 0$, then $\delta m_{c1}, \delta m_{c2}, \ldots, \delta m_{cN} = 0$ and accordingly, $\delta p_{cr} = 0$. Thus, a local optimum has been reached.

APPENDIX 2: NOMENCLATURE

a	radius of the end-ball
$\mathbf{b}$	left eigenvector
c_+	a specified distance between pairs of eigenvalue curves, see equation (17)
$\mathbf{d}$	right eigenvector
F	differential operator defined by equation (10)
F^*	differential operator defined by equation (13)
$\mathbf{F}$	system matrix defined by equation (14)
J	rotatory inertia of the end-ball about an axis through its centre

l_e length of the eth finite element
L total length of the column
$\mathbf{l}$ vector of element lengths defined by equation (19)
$m, m(x)$ mass distribution function
m_i design variables; the mass distribution function evaluated at the nodal points
$\bar{m}_i, \underline{m}_i$ upper and lower bounds on the design parameters
$\mathbf{m}$ design vector with elements m_i
M mass of the end-ball
$\mathbf{M}$ mass matrix
N_e the number of finite elements used
p load parameter
p_{cr} critical load (flutter load)
$\mathbf{Q}_C$ load matrix, corresponding to the conservative part of the loading
$\mathbf{Q}_N$ load matrix, corresponding to the non-conservative (circulatory) part of the loading
$r, r(x)$ radius of the column
$s, s(x)$ stiffness distribution function
$\mathbf{S}$ stiffness matrix
t time
v eigenfunction describing the lateral deflection of the adjoint system
x distance along the column, measured from the clamped end
y eigenfunction describing the lateral deflection of the physical system
ζ dimensionless slenderness parameter defined by equation (9)
κ dimensionless radius-ratio parameter defined by equation (9)
λ complex eigenvalue
μ dimensionless mass of the end-ball
ρ material density of both the column and the end-ball
σ $\mathrm{Re}(\lambda)$; stability parameter
υ dimensionless rotatory inertia of the end-ball
ω, ω_i $\mathrm{Im}(\lambda)$; vibration frequency

Subscripts
$'$ differentiation with respect to the length parameter x
opt refers to an optimal column
uni refers to a uniform column